Cellulose (2026) 33:481–503
https://doi.org/10.1007/s10570-025-06769-4

ORIGINAL RESEARCH

Amidated carboxymethylcellulose: synthesis, characterization and evaluation of their performance in paper coating application

Domenico Santandrea · Jacopo Caldato · Valentina Beghetto

Received: 26 March 2025 / Accepted: 7 September 2025 / Published online: 23 September 2025

Abstract This work reports the first example of the use of octylamine for the functionalization of carboxymethylcellulose (CMC-Oct) to produce highly hydrophobic and oil-resistant paper. CMC functionalization was carried out in water, in the presence of 4-(4,6-dimethoxy-1,3,5-triazin-2-yl)-4-methylmorpholinium chloride (DMTMM) as condensing agent. Different DMTMM/carboxymethylated glucose residues (Glc_{COONa}) molar ratios (0.5, 1, 2.0) were employed to evaluate the efficiency of DMTMM in terms of degree of amidation, measured by ^1H NMR (DA_{NMR}) and Elemental Analysis (DA_{EA}). CMC-Oct with DA_{NMR} of 0.07, 0.14 and 0.24 were obtained and used to prepare films, which were characterised by ATR-FTIR, TGA/DSC, UV–Vis, colour, moisture uptake (MU%) and water vapor permeability (WVP). Best performing film (F2, $DA_{NMR} = 0.24$), was obtained with a DMTMM/Glc_{COONa} molar ratio of 2, giving a reduction in MU% and WVP of 64% and 60% compared to CMC. This formulation (2 wt% in water) was employed for up to three layers of paper coatings. Grammage, thickness, scanning electron microscopy images, contact angle, water vapor permeability (WVP), oil absorption ratio (OAR%), mechanical properties, and surface energy were evaluated and compared among uncoated paper, paper coated with unmodified CMC, and paper coated with CMC-Oct. Data show that three applications of CMC-Oct coating on paper significantly improved the hydrophobicity, barrier, mechanical properties and surface energy of the paper. Contact angles of up to $105 \pm 8°$, significant reduction in WVP and OAR% (up to 56% and 99.8%, respectively), and increase in EB% and TS (+32% and 47%, respectively), supporting its potentials as a sustainable alternative to fossil-based coatings for packaging applications.

Supplementary Information The online version contains supplementary material available at https://doi.org/10.1007/s10570-025-06769-4.

D. Santandrea · J. Caldato · V. Beghetto (✉)
Dipartimento di Scienze Molecolari e Nanosistemi, Università Ca' Foscari Venezia, Via Torino 155, 30172 Venezia, Italy
e-mail: beghetto@unive.it

D. Santandrea
Dipartimento di Architettura e Disegno Industriale, Università Della Campania "Luigi Vanvitelli", Via San Lorenzo-Abazia di San Lorenzo, 81031 Aversa, CE, Italy

V. Beghetto
Consorzio Interuniversitario per le Reattività Chimiche e La Catalisi (CIRCC), Via C. Ulpiani 27, 70126 Bari, Italy

Graphical abstract

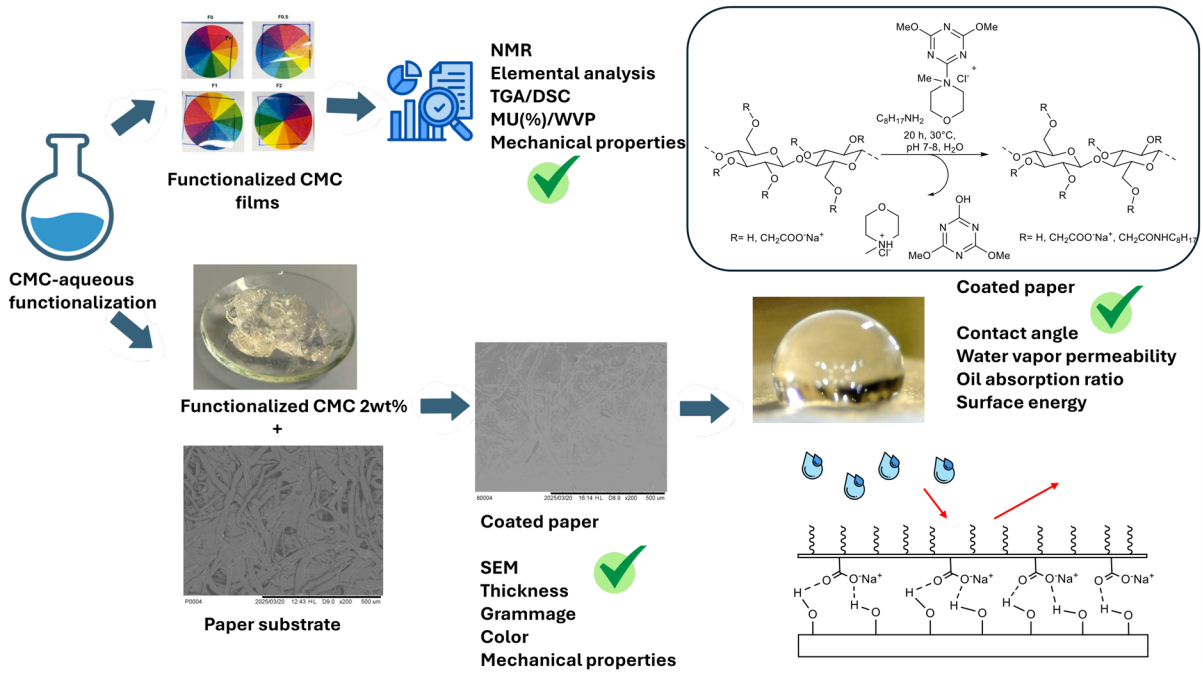

Keywords Carboxymethylcellulose · Polymer functionalization · Amidation · DMTMM · Paper coating · Barrier properties

Introduction

The intensive use of non-biodegradable fossil-based polymers is leading to significant environmental issues, since, due to their chemical and biochemical stability, they accumulate in the environment generating micro and nano plastic pollution (Luo et al. 2024; Ali et al. 2024; Richard et al. 2024). The packaging sector is responsible for the consumption of about 40% of the yearly polymers produced worldwide, as reported by the Plastics Industry Association (Plastics 2025). This includes packaging for food, beverages, consumer goods, and industrial products. Currently, plastic recycling remains limited to only 9% worldwide (UNEP- UN environmental program 2020; Geyer et al. 2017), therefore, there is a growing interest in overcoming these issues by replacing non-biodegradable fossil-based materials with bio-based and biodegradable ones, such as for example paper (Tardy et al. 2023). However, paper has low permeability to water and oil, limiting its potentials (Lavoine et al. 2014; Mujtaba et al. 2022) and coating technology is widely used to improve paper performances and barrier properties (Teisala et al. 2014; de Lima Santos et al. 2024). Conventional strategies often involve the application of fossil-based coatings such as polyethylene, polyvinyl alcohol (PVOH), or acrylic dispersions, which enhance paper barrier performances, but often compromise recyclability (Mujtaba et al. 2022). As a result, there is growing interest in developing bio-based coatings that can improve the functional properties of paper, preserving its recyclability and biocompatibility. Presently different bio-based coatings have been investigated, and they can be divided into solvent and water-based systems. For example, polylactic acid (PLA) and polyhydroxyalkanoates (PHA) can be employed to prepare efficient coatings with good barrier properties, however, their application requires the use of organic solvents, raising concerns about environmental impact and safety (Rastogi and Samyn 2015; Basak et al. 2024).

Water-based bio-coatings, an environmentally friendly alternative, have been prepared from aqueous dispersions of starch, chitosan, and carboxymethyl cellulose (dos Santos Lima et al. 2025; Kunam et al. 2024), however unfunctionalized biopolymer have lack of performances and very often several layers are required for a significant improvement of functional properties. Thus, chemical modification or preparation of composites are required to improve the coating's performance. Consequently, scientific research is highly active in searching optimal balance between coating performance, choice of materials, and mild, sustainable functionalization conditions. (Lavric et al. 2021; Koppolu et al. 2023; Zhang and Youngblood 2025; Swarupa and Thareja 2024). For example, Hassani and coworkers (Hassani et al. 2022) employed citric acid-crosslinked starch applied via impregnation onto alkali-treated paper, followed by hot pressing at 130 °C, achieving notable improvements in hydrophobicity (+68% in water contact angle) and tensile strength (+50%). However, the impregnation method may limit coating uniformity and control over layer thickness. Ni and coworkers (Ni et al. 2018) reinforced starch with zinc nanoparticles, reaching contact angles up to 118°, but the reduction in water vapor transmission rate (WVTR) was modest (12%). Zhang and coworkers (Zhang et al. 2021) reported a 72% reduction in WVP and mechanical enhancements using acetylated cellulose and cinnamaldehyde, however, the acetylation process requires harsh reaction conditions. Similarly, Li and coworkers (Li et al. 2020) functionalized chitosan with castor oil linked by isophorone diisocyanate, achieving moderate barrier improvements, but with no gain in tensile strength and reduced elongation at break.

Building on previous advancements in biopolymer functionalization for paper coatings, this study focuses on carboxymethylcellulose (CMC) and exploring its potentials to enhance paper performances through targeted chemical modifications. In particular, the hypothesis of this study is that CMC can be modified by functionalization with a long alkyl chain amine to improve its hydrophobicity and water vapor barrier properties, making it suitable for paper coating applications. In fact, Charpentier and coworkers (Charpentier et al. 2005; Charpentier et al. 1997) showed the good potentiality of amidated CMC in terms of superior rheological characteristics of the polymer, although CMC-amine was prepared in organic solvent and in the presence of dimetylaminopiridine and dicyclohexylcarbodiimide (DCCI) as condensing agent. Additional strategies have been reported in the literature for the preparation of amidated CMC (Zabivalova et al. 2003; Taubner et al. 2015) however, all foresee the use of organic solvents (methanol, xylene or dimethylformamide DMF), high temperatures and long reaction times. Thus, despite the demonstrated potential of amidated CMC, there remains a gap in the literature regarding mild, fully aqueous-phase amidation approaches specifically aimed at developing functional coatings for paper, leaving an opportunity to explore sustainable processes.

In this work a protocol was tested for the functionalization of CMC with octylamine (CMC-Oct) in water and in the presence of 4-(4,6-dimethoxy-1,3,5-triazin-2-yl)-4-methyl-morpholinium chloride (DMTMM) (Kunishima et al. 1999; D'Este et al. 2014). In fact, DMTMM is a greener condensing agent compared to traditional systems (carbodiimides) since it can be used in water and byproducts formed (2-hydroxy-4,6-dimethoxy-1,3,5-triazine (DMTOH), *N*-methylmorpholinium chloride (NMMCl), Scheme 1) are nontoxic and easily removable by dialysis (D'Este et al. 2014). First, the functionalization efficiency of DMTMM was tested at variable DMTMM/carboxymethylated glucose residues (Glc_{COONa}) molar ratios and degree of amidation measured by NMR and elemental analysis (DA_{NMR} and DA_{EA}). Then, preliminary analysis of the physical mechanical characteristics (ATR-FTIR, UV–Vis, colour analysis, tensile strength (TS) and elongation at break (EB%), DSC, TGA, moisture uptake, water vapour permeability WVP) of CMC-Oct films obtained by casting were performed to select the most promising formulation. In the last part of the work, best performing CMC-Oct formulation was employed for paper coating (from one to three layers). Grammage, thickness, surface morphology, hydrophobicity, colour analysis, WVP, oil absorption ratio (OAR%), EB%, TS, and surface energy of CMC-Oct coated paper were measured and compared to uncoated paper and paper coated with commercially available, unmodified CMC.

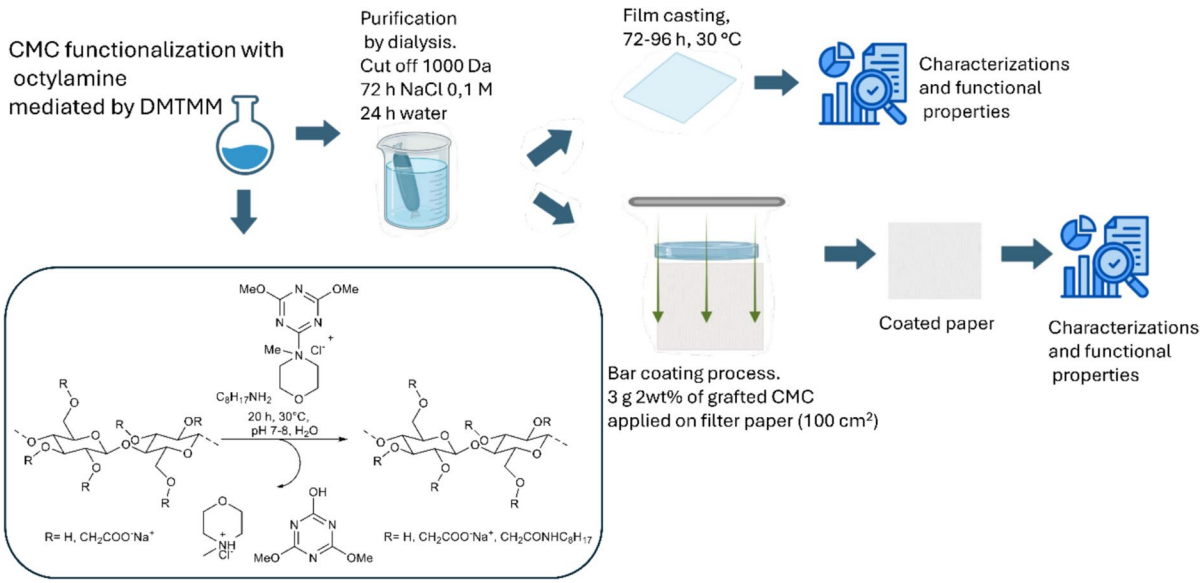

Scheme 1 Chemical functionalization of CMC with octylamine and DMTMM for the preparation of films and coated paper

Materials and methods

Materials

CMC with carboxylation degree DS = 0.7 and average molecular weight 90,000 Da, octylamine, filter paper (Whatman™, Cat No 1113 150, grammage of 125 g/m^2) and DMTMM were purchased from Sigma-Aldrich Co. (St. Louis, MO) and used as received.

Table 1 Sample formulation

Sample	Glc_{COONa}/DMTMM
F0	1/0
F0.5	1/0.5
F1	1/1.0
F2	1/2.0

Each experiment was performed with Glc_{COONa}/Octylamine molar ratio of 1

Methods

Amidation of carboxymethylcellulose

Condensation of CMC and octylamine mediated by DMTMM as a condensing agent was achieved in water to yield the corresponding CMC amide derivative (see Table 1). For example, film F1 was prepared according to the following procedure: 0.5 g of CMC (1.60 mmoles of Glc_{COONa} groups) were solubilized in 20 mL of distilled water. Meanwhile, a solution was prepared containing 10 mL of water, 206.4 mg of octylamine (1.60 mmol, COONa/octylamine 1/1), neutralized with HCl 0.1 M to pH 7 (the final volume after acid addition was adjusted to 20 mL), and 441.6 mg of DMTMM (1.60 mmol, octylamine/DMTMM 1/1); this solution was added to CMC solution and the whole system was left under mechanic stirring at 500 rpm for 20 h at 30 °C. Before adding DMTMM, the pH was carefully controlled using a XS pH 8 Standard Table pH Meter. The acid was added dropwise, with the pH being monitored after each addition. The viscous solution obtained was dialyzed with a 0.1 M sodium chloride water solution for three days and with distilled water for two days, changing the water in 120 min interval using a dialysis tube with cut off 1000 Da. The use of NaCl was necessary to disrupt ionic interactions between the ammonium groups of the amine and the carboxylate groups of CMC (Zhai et al. 2023), while the extended dialysis time ensured complete removal of residual reagents, likely slowed by the increased viscosity of the solution. Control film F0 was prepared as for F1, without the addition of the DMTMM.

Preparation of amidated carboxymethyl cellulose-based films

The obtained solution was transferred into a polystyrene petri dish (9 cm diameter) and oven dried at 35 °C for 48 h. All films were prepared following this procedure with DMTMM/Glc_{COONa} molar ratios reported in Table 1, followed by dialysis and casting. Control sample (F0) was prepared as described for F1 without the addition of the DMTMM. Identification codes of all films prepared in this work are reported in Table 1. A picture of all prepared film is reported in Supplementary Information, Fig. S7.

Characterization of CMC and amidated CMC films

^{1}H, COSY and ^{13}C NMR Spectral analysis

The NMR spectra were recorded using a Bruker Advance 300 spectrometer (Milano, Italy) operating at 298 K and at a frequency of 300.13 MHz for the proton spectrum and 75.4 MHz for the carbon spectrum, chemical shifts were reported on a δ-scale (ppm). The degree of amidation DA_{NMR} was determined from the ^{1}H NMR spectra of CMC by treating 50 mg of film sample with 0.5 mL of deuterated water and 0.5 mL of deuterium chloride at 95 °C for one hour. Chemical shifts (ppm) of CMC in D_2O/DCl have been set as reported by Ho and Klosiewicz (1980). The degree of amidation was calculated according to Eq. (1) (Thompson et al. 2005) for all films.

$$\mathrm{DA} = \frac{\mathrm{I}_{0.93\mathrm{ppm}}/3}{\mathrm{I}_{4.8-5.6\mathrm{ppm}}} \tag{1}$$

where $I_{0.93\ ppm}$ is the area of the signal of the terminal methyl groups in octylamine and $I_{4.8–5.6\ ppm}$ is the area of the anomeric proton (Fig. 1b).

The efficiency of DMTMM was expressed as the ratio between degree of amidation determined by NMR (DA_{NMR}) and theoretical degree of amidation (DA_{th}), according to Eq. (2) for F1 and F0.5 and according to the Eq. (3) for F2(Thompson et al. 2005:

$$\text{DMTMM Efficiency } (\%) = \frac{DA_{NMR}}{DA_{(th)}} * 100 \tag{2}$$

$$\text{DMTMM Efficiency } (\%) = \frac{DA_{NMR}}{DA_{(th)} * 2} * 100 \tag{3}$$

where 2 is the DMTMM/Glc_{COONa} molar ratio.

The amide content is the ratio between the amide carbonyl groups and the total carbonyl group in the CMC and was calculated as reported in Eq. (4) (Thompson et al. 2005):

$$\text{Amide content } (\%) = \frac{DA_{NMR}}{0.7} * 100 \tag{4}$$

where DA_{NMR} is the degree of amidation obtained by NMR and 0.7 is the DS of carboxymethylation of the commercial CMC.

Elemental analysis

Elemental analyses (CHN) were performed using the Unicube Organic Elemental Analyser (Unicube, Lomazzo (CO)), and data reported are the mean values of three replicates. Each sample was performed in triplicate. Degree of amidation by elemental analysis (DA_{EA}) was calculated from these data using an equation present in the literature (Bendahou et al. 2015) reported in the Eq. (5):

$$DA_{EA} = \frac{11.57\%N}{1 - \%N(n + 0.857)} \tag{5}$$

where %N is the nitrogen content in functionalized CMC and n is the alkyl chain length of grafted moieties.

Attenuated total reflectance-fourier transform infrared (ATR- FTIR) spectral analysis

ATR-FTIR spectra of all CMC films were recorded on a FT-IR Perkin-Elmer 1720X spectrometer (Milano, Italy) in Attenuated Total Reflectance (ATR). The ATR-FTIR spectra were collected with a resolution of 2 cm^{-1} in the range of 4000–650 cm^{-1}. Thus, 32 scans were acquired within this interval with at least duplicates for each sample.

UV–Vis analysis and transparency measurements

The UV–Vis spectroscopy analysis of all CMC films prepared were carried out using an Agilent Cary 100 UV/Vis spectrophotometer (Milano, Italy). The films

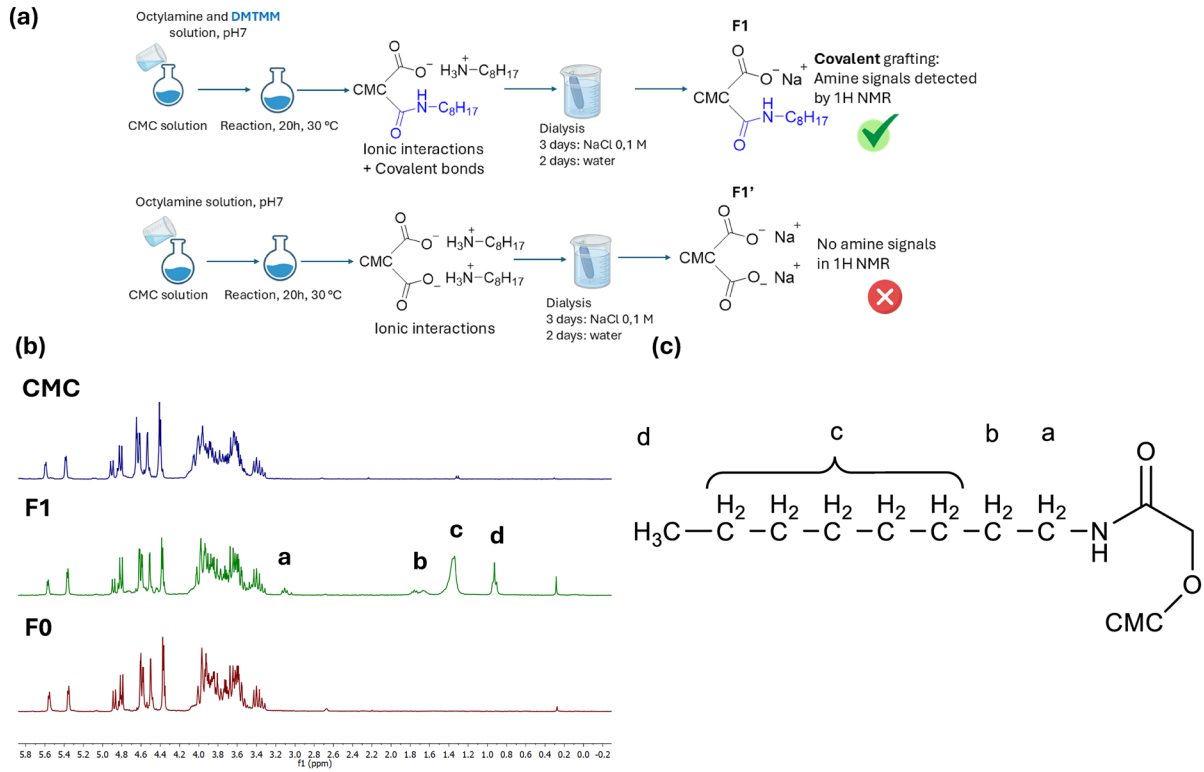

Fig. 1 **a** Experimental procedure for the detection of covalent bond by comparison with blank reaction; **b** ^{1}H NMR spectra of CMC, F1, F0; c) Proton assignment in bonded octylamine

were placed directly into the spectrophotometer test cell and air was used as reference. The optical absorbance of the films was measured in the wavelength range of 200–800 nm with a scan rate of 600 nm/min.

Colour analysis

Colour of all coated paper was evaluated using a portable spectrophotometer CM-26dG (Konica Minolta sensing Inc., CM 2600d, Osaka, Japan) equipped with D65 standard illuminant, specular component excluded mode was used. The results were expressed as L^* (lightness), a^* (redness), b^* (yellowness) and for coated paper Gloss (8°), using a white plate as standard ($L^*=91.76$, $a^*=4.12$, $b^*=-10.9$). All measurements were performed in triplicate on three random locations for each film or paper sample. The total colour difference (ΔE), Yellow Index (YI) and White Indec (WI) were calculated according to Eqs. (6–8):

$$\Delta E = \sqrt{(L_s^* - L^*)^2 + (a_s^* - a^*)^2 + (b_s^* - b^*)^2} \quad (6)$$

$$YI = \frac{146.86xb*}{L*} \quad (7)$$

$$WI = 100 - [(100 - L^*)^2 + a^{*2} + b^{*2}] \quad (8)$$

Differential scanning calorimetry (DSC) and thermal gravimetric analysis (TGA)

DSC analysis of all films was performed on a DSC 3 (Mettler Toledo, USA). The instrument was calibrated using indium as the standard. CMC samples (about 5.0 mg) were weighed into an aluminium oxidized melting pot, sealed and heated from 30 to 500 °C at a heating rate of 10 °C/min. A sealed melting pot filled with Al_2O_3 (about 7.0 mg) was used as the reference. TGA analyses of all films (about 10 mg) were carried

out on a STA PT-1000 (Linseis, Germany) from 30 to 500 °C at the rate of 10 °C/min under nitrogen flow of 50 mL/min.

Mechanical properties of films and coated paper

Mechanical properties of films (F0-F2, see Supplementary Information, Table S3), coated (P1-P3, Table 3) and uncoated paper samples (U1-U3, Table 3) were characterised by TS and EB% as following. The paper and film samples were conditioned at 23 °C ± 1 °C and 50% relative humidity for 48 h. The mechanical tests were conducted using Universal Testing Machine (UTM, Lonos Test Tenso-Test model), equipped with a load cell and displacement control system. Specimens were cut into standard dimensions of 30 mm (paper) and 15 mm (film) width and 80 mm length. The tests were performed at a crosshead speed of 5 mm/min. The tensile strength (MPa) was calculated by dividing the maximum applied force (F, N) at break by the initial cross-sectional area (A, mm^2) of the sample (Eq. 9).

$$TS = \frac{F}{A} \tag{9}$$

The elongation at break was determined as the maximum extension (in percentage) of the sample before rupture (Eq. 10)

$$EB\% = \frac{\Delta l}{l_0} * 100 \tag{10}$$

where Δl is the maximum increment of length before rupture and l_0 is the starting length of the sample. Each measurement was performed in triplicate.

Moisture uptake (MU%)

All CMC films (20 mm × 20 mm) were first conditioned with a saturated solution of K_2SO_4 (RH = 97%) or $MgNO_3$ (RH = 55%) (W) and then dried until constant weight was achieved (W_0). All measurements were performed in triplicate. The moisture uptake (MU%) at two different RH (55% and 97%) values has been calculated according to Eq. (11):

$$MU\% = [(W - W_o) \times 100]/W_o \tag{11}$$

Water vapor permeability (WVP)

WVP tests were carried out according to the ASTM standard method (ASTM E96-95). Cups containing anhydrous CaCl2 (RH = 0%) with an average diameter of 3.5 cm and a volume of 70 mL, were used to determine the WVP of the films. Each cup was covered with a film, paper or coated paper sealed with high vacuum grease and placed in a conditioned desiccator with RH = 75% using saturated sodium chloride. Cups were weighed every 1 h for the first 10 h and finally after 25 h. The water vapor permeability (WVP) was calculated from the WVTR (the slope of increase in weight over time (g/s) divided by the exposed film area (m^2)), the thickness of the sample, the saturation vapor pressure and the relative humidity according to Eq. (12) (10^{-10} g m^{-1} s^{-1} Pa^{-1}):

$$WVP = (WVTR \times t)/[P(R_1 - R_2)] \tag{12}$$

where *t* is film thickness (m), P is the saturation vapor pressure (Pa) at 25.0 ± 2 °C, R_1 is the RH in the room (0.75) and R_2 the RH in the cup (0). Under these conditions, the driving force [$P(R_1–R_2)$] is 1753.55 Pa, expressed as water–vapor partial pressure (Zolfi et al. 2014). All measurements were performed at least in duplicate.

Application in paper coating

The CMC-Oct gel was coated on one sides of the paper using a No.2 wire bar with the wire size of 0.15 mm (RK PrintCoat Instruments Ltd., UK). Each paper sample of 100 cm^2 was coated with 3 g of 2wt% of CMC-Oct for each application. The drying process was carried out at room conditions (a temperature of 25 ± 3 °C and relative humidity of 50 ± 10%) for 48 h, and further oven-dried at 60 °C for 12 h (Tanpichai et al. 2020). Different deposition layers were applied (1 to 3) in order to study its impact on hydrophobicity and barrier properties of the paper. Unmodified-CMC coated papers, obtained as described for modified CMC, were used as control sample.

Film, paper and coated paper thickness

Thickness of the samples was measured with a Digimatic Indicator (Mitutoyo, Japan) having a sensitivity of ± 0.001 mm. Measurements were made at

different points (at least eight) on the same sample (at 25 ± 2 °C, RH = 55%) and average values were calculated between at least eight values.

Grammage of the coating

Grammage of the coating on paper substrate was measured according to the Eq. (13):

$$\text{Grammage}\ (\frac{g}{m^2}) = [(W_c - W_o)]/A \tag{13}$$

where W_c is the weight of the paper after the coating (g), W_0 is the weight of the paper before the coating (g), and A is the area of the paper sample (m^2). Each measurement was performed at least in duplicate.

Scanning electron microscopy

The structure and morphology of the coating on the paper were observed through the TM3000 Tabletop Microscope (Hitachi, Japan) with an acceleration voltage of 15 kV. A sample was mounted on a stub with a double-sided carbon tab and was subsequently coated with a thin gold layer using a sputter coater (108 auto, Cressington Scientific Instruments Ltd., UK) before observations.

Contact angle (θ) measurements

Contact angle measurements were performed using a Celeston Digital Microscope (USA). A drop of 10 µL was placed in contact with the coated and uncoated paper and contact angle value was recorded after drop stabilization (10 s). All measurement were performed at least in duplicate. Picture was processed using ImageJ software for contact angle measurement.

Oil absorption ratio (OAR%)

Paper samples (4 cm diameter) were fixed with parafilm on the top of a glass test tube containing 5 mL of sunflower oil and were placed on the filter paper (previously oven dried at 50 °C until constant weight was reached) upside down for 5 min. Then, the filter paper was weighed, and oil absorption ratio (OAR%) was calculated according to Eq. (14):

$$\text{OAR\%} = (\text{m} - m_o)/m_o \times 100 \tag{14}$$

where m is the weight of filter paper in grams, m_0 is the exposed area. Each measurement was performed at least in triplicate.

Surface Energy Calculation

Surface energy of coated paper was measured using both contact angle measurements and dyne test pens, to obtain complementary quantitative and qualitative data. Two probe liquids were used: water (polar; $\Upsilon_L^p = 51.2\frac{mJ}{m^2}; \Upsilon_L^d = 21.8\frac{mN}{m^2}$) and diiodomethane (non-polar; $\Upsilon_L^p = 0\frac{mJ}{m^2}; \Upsilon_L^d = 50.8\frac{mJ}{m^2}$). The surface energy was determined by the Owen-Wendt method using its linear form (Eq. 15).

$$\Upsilon_s^d = b^2; \Upsilon_s^p = a^2; x = (\frac{\Upsilon_L^p}{\Upsilon_L^d})^{\frac{1}{2}}; y = \Upsilon_L(1 + \cos(\theta))/[2\left(\Upsilon_L^d\right)^{\frac{1}{2}}] \tag{15}$$

where Υ_L is the total surface tension of the liquid, Υ_L^p is the polar component of the liquid surface tension, Υ_L^d is the dispersive component of the liquid surface tension, θ is the contact angle of the testing liquid, Υ_s^d is the dispersive component of the solid surface energy and Υ_s^p is the polar component of the solid surface energy. The total surface energy of the solid surface is given by the sum of polar and dispersive components. In parallel, dyne test pens (38 mJ/m^2) were used. A continuous line of test ink was applied to the surface, and the wetting behaviour was observed for 2 s. A stable line indicated sufficient surface energy, while absorption implied lower energy. This method served as a quick verification of the critical surface tension required for adequate printability.

Statistical analysis

Statistical analysis on multiple samples tested are reported. Average values ± standard deviation was calculated using a one-way and two-way analysis of variant (ANOVA) by means of OriginPro 2019 software. Differences among mean values were processed by the Tukey's multiple range test. Significance was defined at $p < 0.05$. All experiment were performed in triplicates.

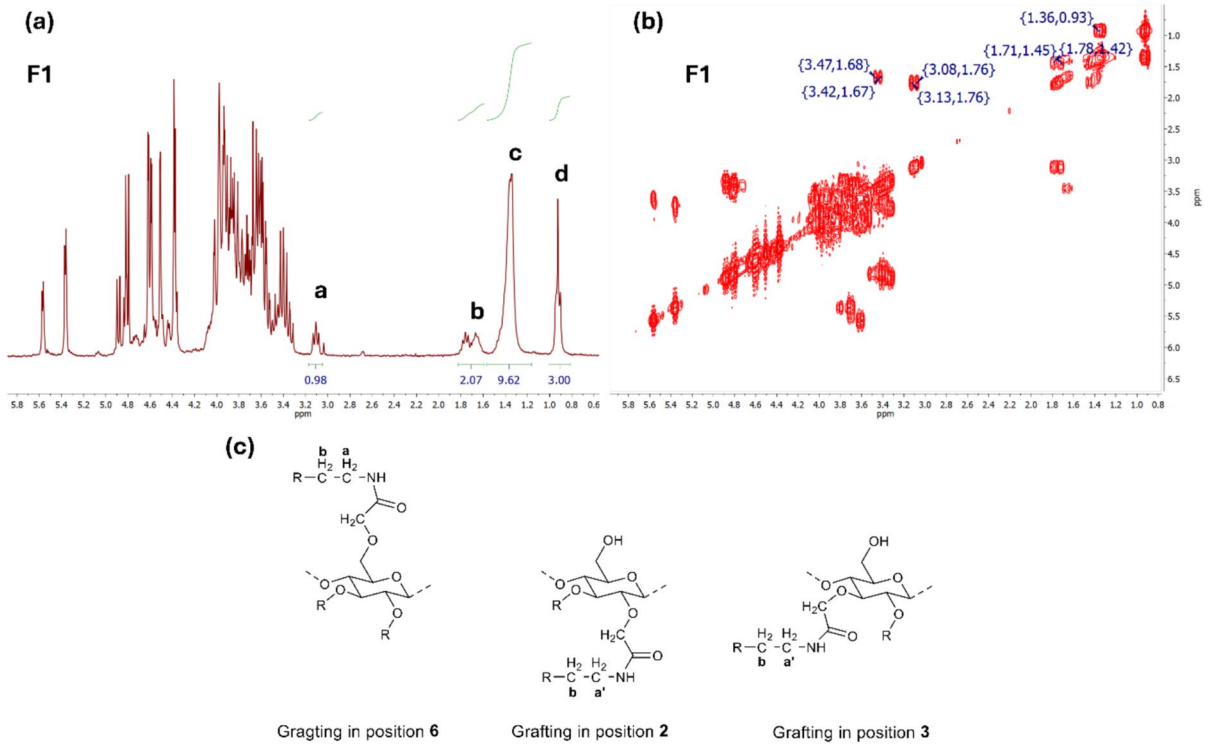

Fig. 2 **a** ^{1}H NMR and **b** COSY NMR of F1; **c** Graphical visualization of different octylamine functionalization position

Results and discussion

Amidated CMC

The amidation reaction between CMC and octylamine was tested in the presence of DMTMM as condensing agent (Scheme 1). Octylamine was chosen as model reagent for CMC functionalization since it is water soluble between pH 7 and 8 and has a relatively long alkyl chain which should improve CMC hydrophobicity (D'Este et al. 2014; Borke et al. 2015; Heydari et al. 2025). DMTMM promotes the reaction in very mild conditions, activating CMC carboxylate groups to the selective attack of an amine, even in a nucleophilic solvent such as water (D'Este et al. 2014; Kunishina et al. 1999, Beghetto et al. 2019; Sole et al. 2021; Santandrea et al. 2025).

Thus, DMTMM allows to carry out the reaction in water, avoiding solvent exchange steps required with other condensing agents commonly employed for amidation reactions on cellulosic materials (Zabivalova et al. 2003; Taubner et al. 2015; Charpentier et al. 1997). Purification from DMTMM byproducts and excess of octylamine was easily performed by dialysis.

One of the main difficulties encountered when cellulosic materials are functionalized is to prove whether covalent, ionic or other weaker interactions are formed and responsible for physical mechanical changes (Pescheux-Sergienko et al. 2024). For this reason, preliminary experiments were carried out with and without DMTMM, in order to verify the efficiency of the condensing agent (Table 1).

Thus, two samples were prepared adding 500 mg of CMC (1.60 Glc_{COONa} mmol) to 20 mL of water. To these solutions, 10 mL of an amine solution (octylamine/Glc_{COONa} moles ratio 1, pH 7) (F0) and 10 mL of an amine/DMTMM solution were added (445.5 mg, DMTMM/Glc_{COONa} moles ratio 1, pH 7) (F1) (Table 1 and Fig. 2a).

Both solutions were left to stir at 30 °C for 20 h, dialyzed to remove DMTMM byproducts and the excess of octylamine, cast and analysed by NMR with the method reported by Ho and Klosiewicz (1980).

Table 2 DA_{th}, DA_{NMR}, DMTMM efficiency, elemental analysis and DA_{EA}

Sample	Yield (%)[a]	DA_{th}[b]	DA_{NMR}[c]	$DMTMM_{eff}$ (%)[d]	Amide content (%)[e]	C(%)[f]	H(%)[g]	N(%)[h]	DA_{EA}[i]
F0	–	–	–	–	–	33.8	5.0	–	–
F0.5	70	0.35	0.07	20	10	37.0	5.4	0.4	0.05
F1	70	0.70	0.14	20	20	41.3	6.0	1.4	0.18
F2	80	0.70	0.24	17	34	45.0	6.4	1.8	0.25

(a) Yield(%) was calculated as the mass ratio between the recovered product and the total amount of starting CMC and octylamine. (b) DA_{th}:theoretical degree of amidation. (c) DA_{NMR}: degree of amidation calculated by NMR. (d) $DMTMM_{eff}$: see materials and method section. (e) Amide content: % of amide group in CMC. (f) C(%): carbon content by elemental analysis. (g) H(%): hydrogen content by elemental analysis. (h) N(%): nitrogen content by elemental analysis. (i) DA_{EA}: substitution degree calculated by elemental analysis

NMR spectra

CMC-Oct was characterized by ^{1}H, COSY NMR and ^{13}C NMR. Considering the ^{1}H NMR spectra of F0 (see supplementary information, Fig. S1), the absence of octylamine signals is evident, while these signals are visible in the ^{1}H NMR spectra of F1 (Fig. 1b), confirming the role of DMTMM in the formation of covalent bond (Fig. 1). In particular, in the ^{1}H NMR spectra of F1 the four signals between 5.6 and 4.8 are assigned to the anomeric proton of the glycosidic ring (α-substituted, α-unsubstituted, β-substituted, β-unsubstituted) (Ho and Klosiewicz 1980), while those between 4.6 and 4.3 ppm are due to the carboxymethyl protons, having different chemical shifts according to the position of the carboxymethyl moieties on the glycosidic ring (Heinze and Pfeiffer 1999). Signals between 4.2 and 3.3 ppm correspond to the glycosidic protons, while the amine protons are present at lower ppm (H_a at 3.1 ppm, H_b two signals between 1.8 and 1.6, H_c at 1.4 and H_d at 0.9 ppm, Fig. 1c).

Interestingly, two unexpected features were evidenced from the ^{1}H NMR spectra of F1. First, setting the integral of H_d to three, H_a integrates 1 instead of 2 (Fig. 2a). Second, a split of the signal assigned to H_b protons is evidenced, which is not present in the ^{1}H NMR and COSY spectra of free octylamine (see Supplementary Information, Figs. S2, S6). In order to better understand this phenomenon COSY experiments were further performed on F1 (Fig. 2b).

The COSY spectrum shows a signal at [3.10, 1.75] ppm due to the coupling between H_b and $H_{a,}$ and surprisingly, an additional new signal at [3.45, 1.68] ppm which was not visible in the mono dimensional ^{1}H NMR spectra appear corresponding to H_a, (Fig. 2b). Different chemical shifts of H_a and H_a, are attributed to the functionalization of the amine on the different carboxymethyl groups of the glycosidic ring (position 2, 3 or 6). H_a is associated with the methylene group of octylamine functionalized in position 6 (lower ppm), while H_a, is assigned to the methylene group of octylamine functionalized in position 2 and 3. This assignment justifies the low integral value of H_a in the mono dimensional ^{1}H NMR spectra. This phenomenon may also explain the splitting of H_b, which also has slightly different chemical shifts due to the position of the functionalization. ^{13}C NMR spectra of F1, as representative sample, is reported in Fig. S5 (supplementary information). The carbon signals of the functionalized octylamine are visible between 10 and 40 ppm, while those of CMC are present between 50 and 100 ppm. Finally, the signals around 170 ppm are assigned to the carbonyl groups.

Based on this findings further experiments were performed with an Octylamine/Glc_{COONa} molar ratio 1/1, and DMTMM/Glc_{COONa} molar ratios of 0.5 and 2.0. After 20 h at 30 °C, all solutions were dialysed, casted to obtain F0.5, F1 and F2 films respectively (Table 1) and characterised as described below.

DA_{NMR} values of the films after functionalization, calculated as the ratio between the integral of H_d and that of the anomeric proton for the glycosidic moieties (4.8–5.6 ppm), were found to be between 0.05 and 0.24 (see supplementary information, Fig. S2, S3). DA_{NMR} values allowed to determine the efficiency of DMTMM (see Eq. 2 and 3), which was found to be around 20% for F0.5 (DMTMM/Glc_{COONa} molar ratio = 0.5) and F1 (DMTMM/Glc_{COONa} molar ratio = 1), moderately decreasing to 17% for

F2 (DMTMM/Glc_{COONa} molar ratio = 2), in agreement with the literature (Cozens et al. 2021). For this reason, DMTMM/Glc_{COONa} molar ratios > 2 were not further investigated. It can be hypothesized that the relatively low degree of substitution is partly attributable to steric hindrance from the bulkiness of the alkylamine side chain, which may limit accessibility to the activated carboxyl groups along the CMC backbone. Furthermore, the amidation occurs via an active ester intermediate formed by nucleophilic attack of the carboxylate on the triazine ring of DMTMM. This intermediate is prone to hydrolysis by water, which, while potentially reducing amidation efficiency, allows straightforward removal of triazine residues and preparation of polymers free from residual organic reagents, in contrast to other condensation agents such as EDC/NHS (Yoshikawa et al. 2025).

Additional information on the conversion of CMC carboxylate groups was determined calculating the percentage of amide content in F0.5, F1, F2, measured as the ratio between DA_{NMR} and the substitution degree of CMC (see Eq. 4 and Table 2) (Thompson et al. 2005). The amide content evidences that, although the overall efficiency of DMTMM remains almost equivalent for all samples prepared, the content of amine bonded employing higher quantities of DMTMM increases (respectively 10% for F0.5, 20% for F1 and 34% for F2).

Elemental composition

Elemental analysis measurements were also performed to calculate DA_{EA} (see Eq. 5) and CHN values of all the samples are reported in Table 2. As expected, nitrogen content increased for samples prepared with higher DMTMM/Glc_{COONa} molar ratios (F0: 0%; F0.5; 0.4%; F1: 1.4%; F2: 1.8%), together with carbon and hydrogen content, as a consequence of the higher degree of CMC functionalization. Interestingly, DA_{EA} values are very similar to those calculated by NMR, confirming the reliability of NMR data.

Amidated CMC-Based films

ATR-FTIR spectra

CMC-Oct solutions prepared as reported above, were used for the preparation of films by casting technology. The aim was to study the influence of amine functionalization on CMC films performances, before moving on to study the applicability of CMC-Oct as coatings for paper applications. ATR-FTIR analysis evidenced the presence of amide carbonyl signals at 1650 cm^{-1} (film F2, Fig. 3a), confirming the functionalization of octylamine on CMC (Le Gars et al. 2020; Sole et al. 2022; Santandrea et al. 2025). Additionally, two new and intense signals at 2927 cm^{-1} and 2857 cm^{-1} were assigned to the C–H stretching of the alkyl chain bonded on CMC. Finally, the signal at 1260 cm^{-1} was attributed to C–N stretching between the nitrogen atom of octylamine and the adjacent methylene group.

UV–Vis and colour analysis

UV–Vis analysis of CMC and CMC-Oct films is reported in Fig. 3b. The absorbance profiles of the functionalized films (F0.5, F1, F2) are comparable to the unmodified CMC film (F0) in the 400–800 nm range, indicating that no significant changes in light absorption occurred upon functionalization.

Importantly, no yellowing was observed (Supplementary Information, Fig. S7), which is significant, considering that CMC typically undergoes visible yellowing when amidation is performed at high temperatures (Lavoine et al. 2016). In contrast, the mild reaction conditions employed here using DMTMM effectively prevent such colour changes. To further support these observations, colorimetric parameters (L*, a*, b*, ΔE), together with the Yellowness Index (Yi) and Whiteness Index (Wi), were measured for all films (see Supplementary Information, Table S1). All samples exhibited a visually bright and neutral appearance, with only minimal variations across the different degrees of functionalization. The lightness remained consistently high, and colour coordinates confirmed the absence of any relevant colour shift. In particular, the yellowness of the films slightly decreased after functionalization, while whiteness remained unchanged. These results demonstrate that CMC functionalization under the applied conditions does not compromise the optical quality of the films. The visual appearance remains clean, bright, and colour-neutral, making these materials well-suited for applications where transparency is important.

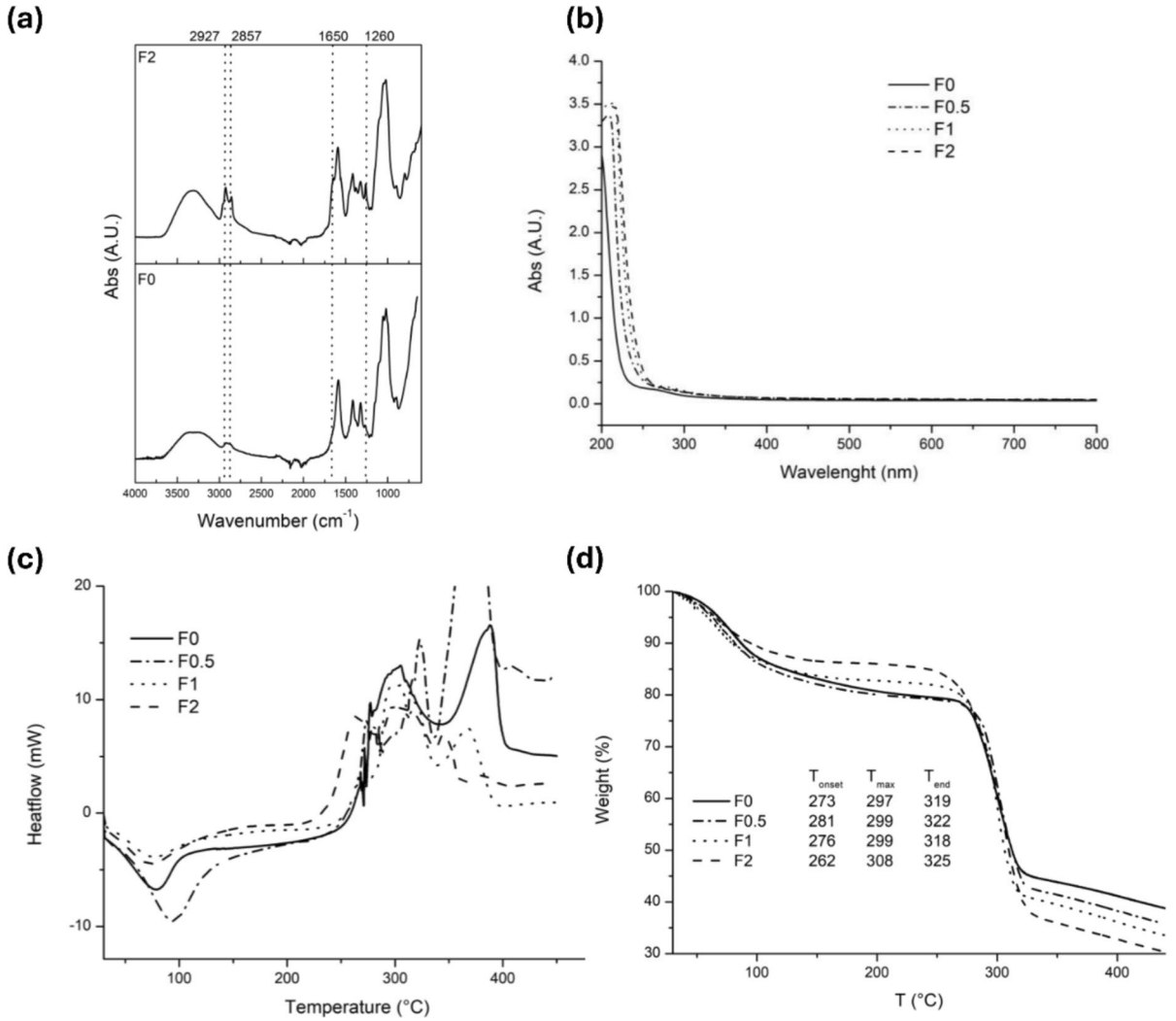

Fig. 3 **a** ATR-FTIR spectra of F0 and F2; **b** Abs graphs in the range 200–800 nm of F0, F0.5, F1, F2 films; **c** DSC graphs of F0, F0.5, F1, F2; **d** TGA graphs of F0, F0.5, F1, F2

DSC and TGA analysis

Films were also characterised by thermal analysis, such as DSC (Fig. 3c) and TGA (Fig. 3d). DSC analysis showed an endothermic peak around 100 °C assigned to residual moisture evaporation (Riaz et al. 2020) and an intense exothermic peak starting at 250 °C, assigned to decarboxylation and depolymerization of CMC (El-Sayed et al. 2011).

TGA measurements are reported in Fig. 3c, indicating the beginning (T_{onset}), maximum (T_{max}) and end (T_{end}) of the thermal degradation of the different CMC samples, under nitrogen atmosphere. It can be easily seen that, mass loss between 30 and 100 °C is reduced, indicating that decreasing amounts of moisture are present in the samples as the DA increases (Fig. 3c). Interestingly, T_{onset} of films F0 to F2 also decreases, possibly due to a plasticising effect of the alkyl chains of the functionalized amine.

Mechanical properties

Tensile strength (TS) and elongation at break (EB%) of native CMC, CMC treated with DMTMM only (F0) and octylamine-functionalized CMC (F0.5, F1 and F2) are reported in supplementary information,

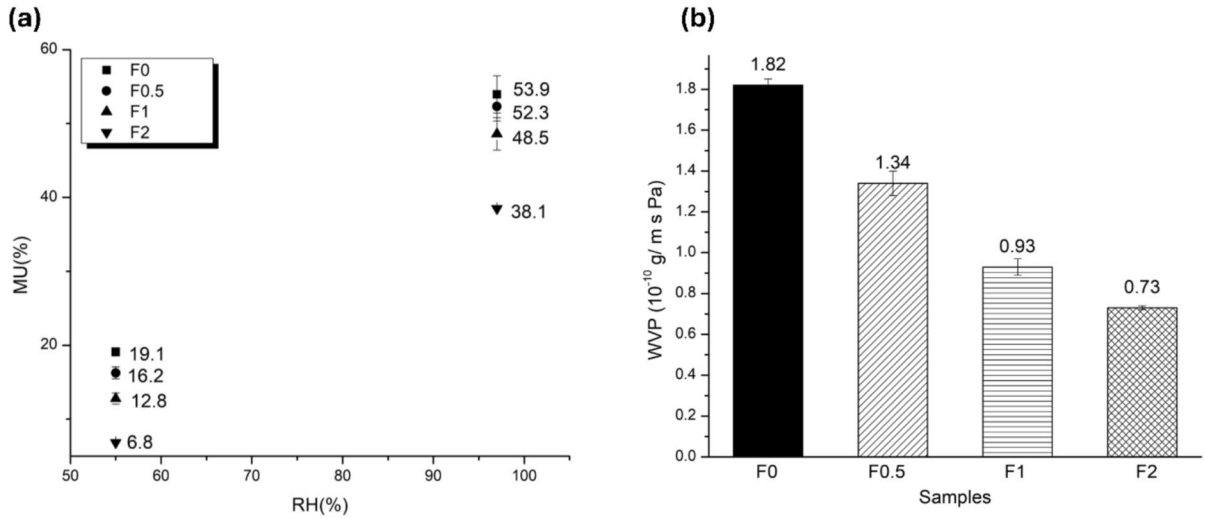

Fig. 4 **a** MU% of F0-F2 **b** WVP (g m^{-1} s^{-1} Pa^{-1}) of F0-F2

Table S3 and Fig. S8. Sample F0, treated with amine alone (no DMTMM), shows mechanical properties nearly identical to the unmodified CMC (53 ± 3 TS, 5.0 ± 0.1 EB), consistent with values reported in the literature (Rachtanapun et al. 2012). In contrast, samples F0.5, F1, and F2 exhibit a marked decrease in tensile strength and variable behaviour in elongation at break. Notably, sample F0.5 shows the largest drop in TS (from 52 ± 2 to 33 ± 2 MPa) and a moderate reduction in EB (3.2% ± 0.1), suggesting structural modification. However, in samples F1 and F2, TS further decreases (to 27 ± 3 and 31 ± 2 MPa, respectively), while EB increases to 5.0% ± 0.2 and 6.0% ± 0.3. The observed trend with decreasing TS and increasing EB is typical of plasticizing effects. This is attributed to the alkyl chain of the grafted amine, which, once attached to the polymer backbone, disrupts intermolecular interactions and increases chain mobility (Pettignano et al. 2019b). As a result, the material becomes more flexible but less resistant to stress.

Water uptake and water vapor permeability

Additionally, MU% and WVP of CMC-Oct films were measured since they are very important parameters, determining the packaging efficiency (Ghanbarzadeh et al. 2010) (Fig. 4 and Supplementary Information, Table S2). MU% was calculated at two different RH (RH = 55% and 97%) in order to study the behaviour of CMC-Oct films in different moisture conditions (Fig. 4a).

Data clearly show a strong dependence of MU% from the DA at both relative humidities tested, and very high performances were obtained with F2, with a reduction up to 64% at RH 55% ($p < 0.05$) and 30% at RH 97%, compared to control sample F0. This is attributed to the presence of the hydrophobic alkyl chain in functionalized CMC. As for MU%, also WVP permeability is greatly affected by the DA and in F2 (0.73 ± 0.01 10^{-10} g m^{-1} s^{-1} Pa^{-1}) it decreased by 60% compared to F(0) ($p < 0.05$) (Fig. 4b, Table S2). This very low WVP further evidences the importance of the presence of a hydrophobic alkyl chain in inhibiting water vapor diffusion through the film (Li et al. 2019).

To the best of our knowledge, no studies have yet reported the functionalization of carboxymethyl cellulose (CMC) followed by film formation and subsequent evaluation of its moisture barrier properties. Thus, literature examples involving the functionalization of nanocelluloses are considered as a comparative framework, allowing to explore how chemical modifications might influence water vapour barrier performance. Surprisingly, in this latter case the presence of a hydrophobic alkyl chain was not always associated with an improvement in WVP. In fact, Solala and coworkers investigated the surface functionalization of cellulose nanofiber films with long alkyl chain epoxides and, despite the decrease

Table 3 Thickness, Grammage, Contact angle, WVP (g m^{-1} s^{-1} Pa^{-1}) and OAR% of coated paper

Sample	Deposition layer	Thickness (μm)	Grammage (g/m^2)	Water contact angle (10 s)	WVP (10^{-9} g m^{-1} s^{-1} Pa^{-1})	OAR%, 5 min (g/m^2)	EB%	TS (MPa)
P0	0	216 ± 10^{a}	0^{a}	–	1.90 ± 0.07	253 ± 1^{a}	3.9 ± 0.7^{a}	57 ± 14^{a}
P1	1	234 ± 26^{a}	4.7 ± 0.3^{b}	93 ± 9^{a}	1.06 ± 0.08	5.7 ± 0.6^{b}	6.7 ± 1.3^{b}	72 ± 2^{b}
P2	2	253 ± 26^{a}	10.0 ± 0.5^{c}	95 ± 6^{ab}	1.02 ± 0.02	2.3 ± 0.7^{c}	6.7 ± 0.1^{b}	72 ± 3^{b}
P3	3	265 ± 20^{ba}	14.9 ± 0.1^{d}	105 ± 8^{b}	0.84 ± 0.08	0.7 ± 0.4^{d}	8.4 ± 0.2^{c}	84 ± 1^{c}
U1	1	225 ± 18^{a}	5.0 ± 0.5^{b}	–	1.95 ± 0.06	277 ± 9^{e}	8.9 ± 0.5^{d}	100 ± 7^{d}
U2	2	235 ± 20^{a}	9.8 ± 0.7^{c}	–	2.12 ± 0.10	210 ± 16^{f}	10.7 ± 0.2^{e}	107 ± 26^{d}
U3	3	240 ± 20^{a}	15.3 ± 0.8^{d}	–	2.32 ± 0.14	164 ± 28^{g}	10.1 ± 0.8^{e}	113 ± 26^{d}

Values given are mean ± standard deviation

Values with different superscripts in the same column are significantly different ($p < 0.05$)

in wettability of the functionalized material, the authors did not observe any improvement in terms of WVTR (Solala et al. 2018). Similarly, Shimizu and coworkers showed that the ionic functionalization of TEMPO-oxidized cellulose nanofibers with quaternary ammonium salts increases WVP, although an improvement in surface hydrophobicity was observed (Shimizu et al. 2014). Only, Li and coworkers found an improvement of about 65% of WVP after chemical functionalization of cellulose nanofibrils with 10-undecylenoyl chloride, in line with results reported in this work (Li et al. 2019). Regarding CMC, there are just few examples on the impact of the crosslinking of CMC on barrier properties (Beghetto et al. 2020; Mu et al. 2012; Nongnural et al. 2024, Hickman et al. 2024; Šimkovic et al. 2023), but more commonly CMC is used in blends with other polymers or as additive (Tavares et al. 2020; Putri et al. 2017; Kim et al. 2021) and no similar functionalization protocols have been reported.

Amidated CMC-coated paper

Best performing CMC-Oct formulation (F2), obtained with a DMTMM/Glc_{COONa} molar ratio of 2 (DA_{NMR} 0.24), was employed for paper coating (2 wt% in water, Fig. S9). Commercially available paper (P0) was bar coated with up to three layers of CMC-Oct (P1, P2 and P3) and data were compared to unmodified-CMC coated paper (U1, U2 and U3) and uncoated paper (P0) (Table 3, supplementary information, Fig. S10). Each deposition corresponds to an increase in grammage of about 5 g/m^2 and to an increase in paper thickness of about 12 μm for P1-P3 and less accentuated for U1-U3. Scanning electron microscopy (SEM) was used to study the surface morphology and images of P0 and coated P1, P2 and P3 samples are reported in Fig. 5a. SEM images evidence that the paper network is gradually filled by the different applications of the coating, leading to the formation of a continuous layer.

In particular, the first two coating applications (P1, P2 Fig. 5a) were not sufficient to completely fill the pores of the paper, while after three applications the paper network is filled and a thin smooth and even film of CMC-Oct is formed. Further pictures and SEM images of the coating on the paper surface are reported in the Supplementary Information section (Figs. S11–S14). In contrast, SEM analysis of the samples coated with unmodified CMC (U1, U2, U3) did not reveal the presence of a continuous film on the paper surface (see Supplementary information, Figs. S15–S17). This is probably due to the higher hydrophilicity and lower molecular interactions of unmodified CMC with paper, which probably penetrates into the paper matrix rather than forming a surface coating. As a result, unmodified CMC does not provide visible surface coverage under SEM observation (He et al. 2021).

Colour analysis

The colorimetric parameters of untreated paper (P0) and coated samples with functionalized CMC (P1, P2, P3) and unmodified CMC (U1, U2, U3) are summarized in Table 4.

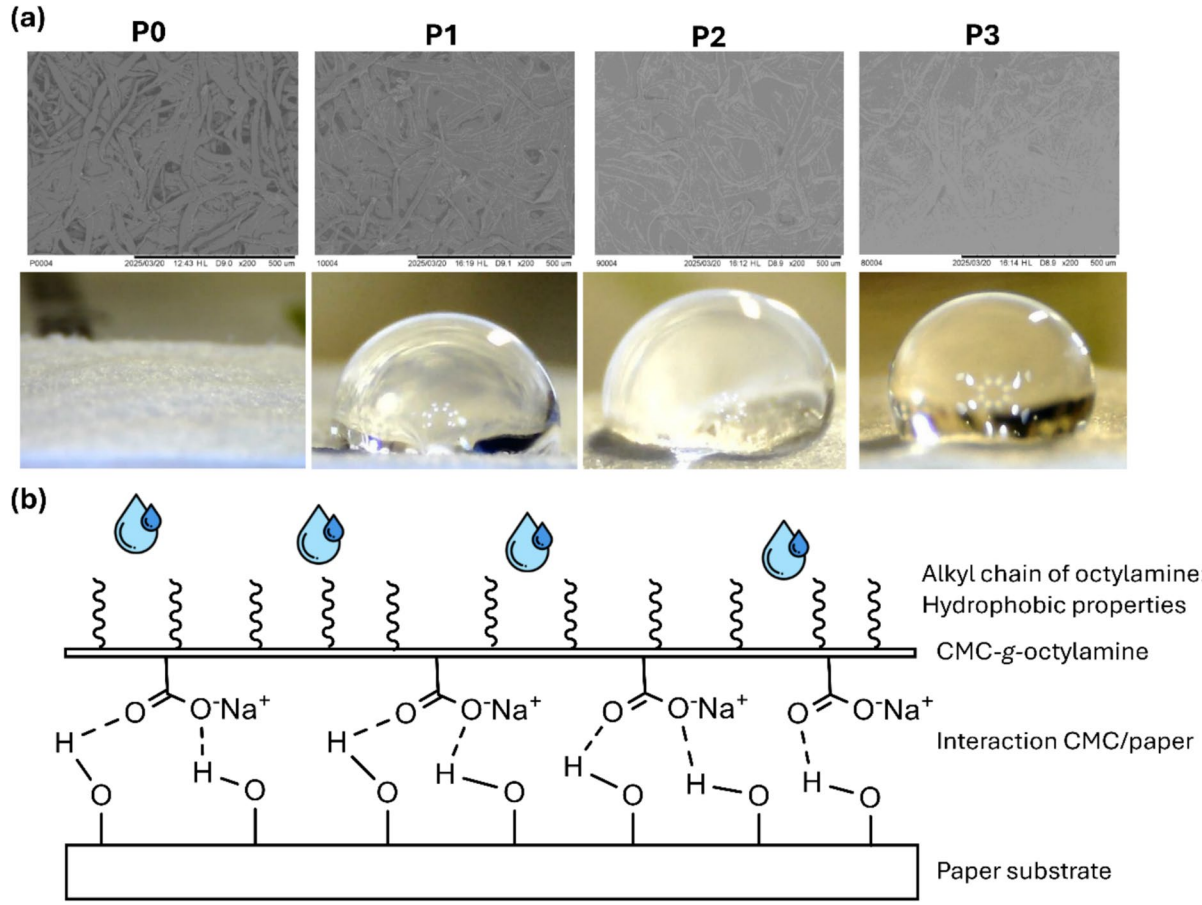

Fig. 5 **a** Scanning electron microscopy (SEM) and contact angle images of P0-P3; **b** Schematic representation of the structure of aminated CMC-based surface coating

Table 4 Hunter colour values (L^*, a^* and b^*), total colour difference (ΔE), yellowness index (YI), whiteness index (WI), of uncoated paper P0, and coated papers P1-P3, U1-U3

Sample	L*	a*	b*	ΔE	Yi	Wi	Gloss (8°)
P0	95.61 ± 0.01^{a}	-0.55 ± 0.01^{a}	1.77 ± 0.03^{a}	6.64 ± 0.01^{a}	2.71 ± 0.05^{a}	95.25 ± 0.02^{a}	14.33 ± 0.58^{a}
P1	94.88 ± 0.21^{b}	-0.54 ± 0.01^{a}	1.95 ± 0.16^{ba}	5.90 ± 0.19^{b}	3.01 ± 0.24^{a}	94.34 ± 0.02^{b}	14.00 ± 0.01^{a}
P2	$94.96 \pm 0,10^{b}$	-0.54 ± 0.02^{a}	2.07 ± 0.17^{b}	5.96 ± 0.08^{b}	3.20 ± 0.26^{a}	94.52 ± 0.14^{c}	16.00 ± 1.00^{b}
P3	95.08 ± 0.10^{bc}	-0.55 ± 0.02^{a}	2.41 ± 0.16^{c}	6.06 ± 0.10^{b}	3.73 ± 0.25^{b}	94.49 ± 0.02	17.00 ± 1.00^{b}
U1	$95.18 \pm 0,12^{c}$	-0.50 ± 0.03^{b}	1.94 ± 0.15^{a}	6.19 ± 0.10^{b}	2.99 ± 0.23^{a}	94.78 ± 0.05^{d}	14.00 ± 0.27^{a}
U2	$94.85 \pm 0,37^{dc}$	-0.49 ± 0.06^{b}	2.13 ± 0.54^{b}	5.85 ± 0.32^{b}	3.30 ± 0.82^{ab}	94.38 ± 0.14^{e}	13.50 ± 0.71^{a}
U3	$94.48 \pm 0,13^{d}$	-0.52 ± 0.01^{b}	2.36 ± 0.11^{b}	5.46 ± 0.12^{c}	3.67 ± 0.17^{b}	93.97 ± 0.07^{f}	13.00 ± 0.05^{c}

Tr: Transparency measured at 600 nm; t: Film thickness (μm)

Values given are mean ± standard deviation

Values with different superscripts in the same column are significantly different ($p < 0.05$)

The untreated paper (P0) exhibits a high lightness value (L* = 95.61 ± 0.01), indicating a bright and clean surface. In coating with CMC-Oct (samples P1, P2, and P3), a slight decrease in lightness is observed (L* ranging from 94.88 ± 0.21 to 95.08 ± 0.10). The a* values remain stable and slightly negative (−0.54 ± 0.01 to −0.55 ± 0.2), indicating no significant changes in the green–red axis.

As the number of layers increases, the b* values show a gradual increase from 1.95 ± 0.16 in P1 to 2.41 ± 0.16 in P3, reflecting a modest increase in yellowness. Correspondingly, the yellow index (Yi) increases from 3.01 ± 0.24 (P1) to 3.73 ± 0.25 (P3). The total colour difference (ΔE) relative to P0 varies between 5.90 ± 0.19 and 6.06 ± 0.10, indicating limited colour changes. Notably, the gloss (8°) increases progressively with coating layers in the modified CMC series, from 14.00 ± 0.01 in P1 to 17.00 ± 1.00 in P3, suggesting the formation of a smoother and more reflective surface.

In contrast, the unmodified CMC coatings (U1, U2, U3) show similar trends in lightness and colour coordinates, with a slight decrease in L* values (from 95.18 ± 0.12 to 94.48 ± 0.13) and an increase in yellowness (b* from 1.94 ± 0.15 to 2.36 ± 0.11; Yi from 2.99 ± 0.23 to 3.67 ± 0.17). However, gloss values in the U series decrease with additional layers (from 14.00 ± 0.27 in U1 down to 13.00 ± 0.05 in U3), possibly indicating a less uniform coating or increased surface roughness.

Overall, while both coating types produce moderate colour changes compared to untreated paper, the modified CMC coatings uniquely enhance surface gloss, which may be advantageous for applications requiring improved aesthetics.

Hydrophobicity

Water contact angle (θ_w) measurements were carried out (Table 3) and three representative pictures of θ_w of P0, P1, P2 and P3 are shown in Fig. 5a. θ_w of control sample P0 is not detectable since the water drop is completely absorbed as soon as it comes in contact with the paper. On the other hand, θ_w of coated samples P1, P2 and P3 significantly improved compared to P0 (respectively 93° ± 9°, 95° ± 6° and 105° ± 8°). An hypotheses of the role of the coating in promoting the hydrophobicity of P0 is reported in Fig. 5b. In line with the literature, polar groups of CMC-Oct establish polar interactions with the hydroxyl groups of the paper, while apolar alkyl chains of the bonded amine should play a key role in the hydrophobization (Yook et al. 2020). Contact angle measurements could not be performed on U1-U3 samples because the water droplet did not stabilize on the coated paper surface but was rapidly absorbed (as for P0 sample).

WVP

WVP measurements were performed on P0–P3 and U1–U3 samples and data are reported in Table 3. Results show that after the first coating application (P1) a decreases in WVP of about 44% was measured compared to P0, while no significant improvement was observed between P1 and P2 samples. An additional improvement was obtained with three coating layers (P3), showing a reduction in WVP of 56% compared to F0 (0.84 ± 0.08 10^{-9} g m^{-1} s^{-1} Pa^{-1}). This is attributed to the formation of a continuous hydrophobic film on the paper surface, as confirmed by SEM analysis, increasing barrier properties of the paper (Zhang et al. 2019). On the contrary WVP of U1–U3 showed an opposite trend, and WVP values increased as the number of unmodified CMC layers increased, due to the hydrophilic nature of CMC, promoting water vapor diffusion through the paper. To summarise, the coating developed in this work lead to a reduction of 44% of WVP at low grammage (4.7 g/m^2, P1, Table 3), and up to 56% WVP reduction with a grammage of 14.9 g/m^2 (P3, Table 3).

In this connection it is important to note that paper coating grammage is particularly relevant in determining its recyclability. In fact, the EU Implementing Directive 2019/665 regarding packaging recyclability reports that “to attain the recycling targets set in former Directive 94/62/EC, composite packaging and other packaging composed of more than one material can be considered recyclable if different material components (plastic coating, lamination) are an insignificant part of the packaging unit, and in no case more than 5% of the total mass of the packaging unit”.

Interestingly, the wt% of one layer of CMC-Oct coating reported in this work is below the maximum weight requirement set for recyclability (3.6 wt%),

and it should further be considered that even for higher coating wt% (P2, 7.4wt% and P3, 10.6 wt%) the similar chemical nature between the coating and the support (paper) should in any case permit recyclability. Further studies are ongoing to verify this hypothesis.

OAR%

Oil absorption ratio (OAR%) tests were also performed on all paper samples (Table 3). In particular, all CMC-Oct coated paper samples showed higher OAR% compared to control sample P0 and one coating application was enough to decrease the OAR% of about two orders of magnitude (P1, Table 3). A gradual improvement of OAR% was further observed for P1 (OAR% = 5.7 ± 0.6) and best performances were obtained for P3 (OAR% = 0.7 ± 0.4, -99.8% compared to P0). In agreement with the literature, this phenomena may be attributed to the formation of a uniform thin film on the paper surface, significantly decreasing the porosity of the paper and consequently improving the OAR% (Mazhari Mousavi et al. 2017; He et al. 2021). As far as the paper samples coated with unmodified CMC are concerned (U1–U3) only a modest improvement in OAR% was observed as the number of coating layers increased. This difference in performance can be attributed not only to the chemical nature of the coatings, but also to their film-forming behaviour. Unmodified CMC, due to its high hydrophilicity and affinity for cellulose fibers, tends to penetrate into the paper structure rather than forming a continuous surface film. As a result, it provides minimal surface coverage and fails to create an effective barrier layer against oil penetration, even when applied in multiple layers.

Mechanical properties

The tensile properties of the coated and uncoated paper samples were evaluated in terms of elongation at break (EB%) and tensile strength (TS) (Table 3 and supplementary information, Fig. S18). P0 exhibited the lowest mechanical performance, with an EB% of 3.9% ± 0.7 and a TS of 52 ± 14 MPa. Upon application of a single coating layer (P1), both EB% and TS increased significantly (EB% 6.7% ± 1.3 and TS 72 ± 2 MPa), and further improvements were observed with additional coating layers. The best-performing sample (P3) reached an EB% of 8.4% ± 0.2 and a TS of 8.4 ± 0.1 MPa. These data demonstrate that the application of CMC-Oct coatings enhances both flexibility and tensile resistance of the paper. The observed improvements are likely due to the formation of a continuous, flexible polymeric film that reinforces the fiber network and distributes mechanical stress more effectively. Notably, the increase in EB% suggests that the coating contributes to ductility without causing brittleness, which is beneficial for packaging applications requiring a balance between strength and flexibility. The slight plateau in TS from P1 to P2 may indicate a saturation of fiber–coating interactions, while the continued rise in EB% for P3 suggests that thicker coatings enhance extensibility at higher coverage levels. Similar trends have been reported in the literature; for example, Kobayashi and coworkers (Kobayashi et al. 2024) demonstrated that CMC-based composite paper sheets exhibited notable increases in EB% and TS, attributed to improved bonding between cellulose fibrils. Interestingly, while the CMC-Oct coatings (P1–P3) improved mechanical properties compared to uncoated paper (P0), the unmodified CMC-coated samples (U1–U3) showed even higher EB% and TS values. This behaviour is attributed to the hydrophilicity of native CMC, which allows deeper penetration into the paper matrix and promotes stronger interactions with cellulose fibers. In contrast, the more hydrophobic CMC-Oct coatings likely form a superficial film with lower affinity for the fiber network. Nevertheless, P1–P3 coatings still provide an evident mechanical reinforcement compared to P0, confirming their potential as dual-function coatings that combine barrier performance with structural enhancement.

Surface energy and printability

Surface energy measurements (Fig. 6) were obtained using the Owens–Wendt method, employing θ_w and diiodomethane contact angle (θ_i) (see Supplementary Information, Table S3 and Figs. S19–S21). P1 exhibited a surface energy of 26 mJ/m^2, while samples P2 and P3 showed higher values, respectively 76 mJ/m^2 and 74 mJ/m^2, corresponding to higher surface energy, mainly attributed to a dominant dispersive component rather than a strong polar contribution (Fig. 6). This suggests that the application of at least two coating applications is required to enhance

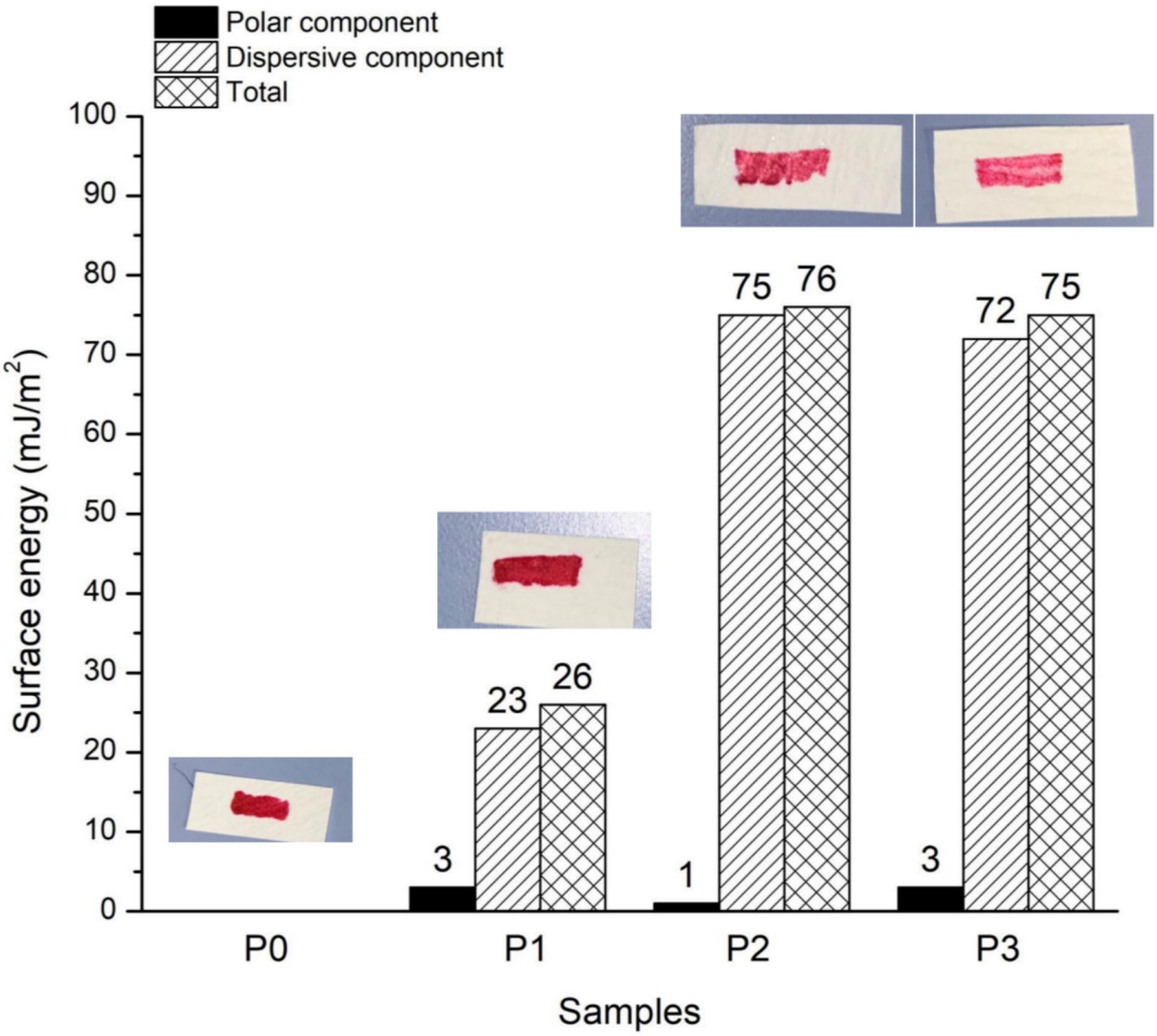

Fig. 6 Surface energy of P0-P3 and Dyne (38 mJ/m^2 test ink) test

van der Waals interactions. In contrast, the much lower surface energy of P1 reflects limited intermolecular interaction potential, likely due to insufficient or uneven coating. The observed predominance of the dispersive component in the surface energy of P2 and P3 can be attributed to the application of octylamine functionalized CMC coating. While this modification reduces the polar character of the surface, it enhances dispersive interactions through the presence of non-polar alkyl groups, leading to high total surface energy values. This behaviour indicates that the coating system is energetically active yet resistant to water absorption, which is advantageous for packaging applications. Dyne level with a 38 mJ/m^2 test ink further supported these findings: P2 and P3 retained continuous ink lines without retraction, confirming that their surface energy exceeds the threshold commonly required for adequate printability. P1, on the other hand, showed ink line diffusion, due to uneven coating (Fig. 6). The correlation between Owens–Wendt results and dyne testing confirms the reliability of combining these two techniques to assess surface characteristics. Overall, P2 and P3 demonstrate surface properties suitable for printing applications. For the control samples U1, U2, and U3 (coated with unmodified CMC), surface energy

assessment was conducted qualitatively, as both water and diiodomethane droplets were rapidly absorbed into the substrate, preventing stable contact angle measurements. In the dyne test, the ink visibly spread and diffused into the surface rather than remaining on top, indicating limited wetting resistance (see Supplementary Information, Fig. S22). This behaviour is attributed to the high hydrophilicity and lack of a continuous barrier layer formed by the native CMC coating on paper.

Literature comparison

Although paper coating applications using CMC are relatively unexplored in the literature, and no prior studies have explored the use of chemically functionalized CMC for this purpose, a few selected works provide useful comparison. Basta and coworkers (Basta et al. 2015) investigated CMC-chitosan composite coatings on paper and observed a significant reduction in water vapor permeability (WVP) of approximately 88% compared to uncoated paper, attributed to electrostatic interactions between cationic chitosan and anionic CMC. However, no notable improvements in mechanical properties were reported within experimental error.

He and coworkers (He et al. 2021) developed a coating based on CMC, cellulose nanocrystals (CNC), and silver nanoparticles, achieving a 45% reduction in WVP. In line with the current study, they also observed improvements in tensile strength (TS) and elongation at break (EB%) upon coating with unmodified CMC. Yet, the inclusion of nanoparticles did not significantly enhance the mechanical performances. Acetylated cellulose has also shown potential in coating applications.

Zhang and coworkers (Zhang et al. 2021) reported a 72% WVP reduction and mechanical enhancements (TS + 33%, EB + 28%) after coating with acetylated cellulose and cinnamaldehyde. However, the preparation required elevated temperatures (60 °C), strong acids, and acylating agents. In comparison, the present CMC-Oct system achieves similarly significant improvements in both barrier and mechanical properties using far simpler processing conditions.

More in general, chemical functionalization or nanocomposite approaches have focused on the chemical functionalization of other biopolymers to enhance coating performance. Ni and coworkers (Ni et al. 2018) developed starch-zinc nanoparticle coatings, reaching contact angles up to 118°, though only a modest 12% WVTR reduction was observed. Again, the performance of the CMC-Oct coatings reported in this paper is superior in terms of barrier efficiency, environmental safety, and processing simplicity. Hassani and coworkers (Hassani et al. 2022) developed coated papers using citric acid-crosslinked starch, prepared by heating the formulation at 90 °C for 5 min. The coating was applied by impregnation onto alkali-treated and bleached paper substrates, which were subsequently hot-pressed at 130 °C to enhance fiber–matrix adhesion. The alkali-treated samples exhibited notable improvements in hydrophobicity (with a 68% increase in water contact angle) and mechanical strength (up to 50% higher than uncoated paper) due to better adhesion thanks to the residual lignin. Nevertheless, the use of impregnation rather than surface film deposition may have limited the homogeneity and thickness control of the coating layer. Finally, Li et al. (2020) functionalized chitosan with castor oil using isophorone diisocyanate as a linker, yielding a moderate 20% reduction in water vapor transmission rate (WVTR) compared to unmodified chitosan-coated paper. Despite improved barrier properties, the coated paper showed unchanged TS and a decrease in EB%. The surface energy of the modified chitosan coating reached 40.87 mJ/m^2 (vs. 43.82 mJ/m^2 for unmodified chitosan).

In contrast, the present work demonstrates that while unmodified CMC (U-series) offers limited barrier performance, exhibiting high hydrophilicity, undetectable water contact angle, and increased WVP, but the introduction of hydrophobic octyl chains via mild functionalization (CMC-Oct) significantly enhances coating performance.

Conclusions

This study presents a novel and fully water solvent based method for the amidation of carboxymethylcellulose (CMC) with octylamine, mediated by DMTMM, to develop hydrophobic, oil-resistant and functional paper coatings. The functionalization efficiency was evaluated through the degree of amidation (DA), determined by both NMR and elemental analysis, with consistent results and a

maximum DA_{NMR} of 0.24 with DMTMM/Glc_{COONa} molar ratio of 2 was obtained. Functionalized CMC films (CMC-Oct) showed reduced moisture uptake and water vapor permeability, especially at higher DA, without affecting optical properties. The best-performing formulation (F2) was applied via bar coating on paper, resulting in notable improvements in hydrophobicity, water vapor permeability, oil resistance and surface energy compared to uncoated samples and control samples. The CMC-Oct coatings slightly decrease paper lightness and increase yellowness but enhance surface gloss compared to unmodified CMC, indicating improved aesthetic properties due to coating coverage. These findings demonstrate the feasibility of producing efficient, hydrophobic, and functional paper coatings using amidated CMC, prepared in mild processing conditions. This work is a preliminary proof-of-concept, laying the foundation for further research aimed at optimizing the process, and scaling up packaging applications. Use of cellulose-based coatings suggests potential compatibility with standard paper recycling processes; nevertheless, further investigations are required to comprehensively assess fiber recovery and recyclability. Future studies should also address additional properties, such as gas permeability, and explore long-term performances. Although the water vapor barrier of biopolymer-based coatings is generally lower than that of fossil-based polymers (e.g., polyethylene), these coatings offer sustainable advantages, including renewability, biodegradability, and potential for functionalization, which justify continued research and development in this field.

Acknowledgments The work was supported by PNRR funding for the 38th PhD cycle "Dottorato di Interesse Nazionale in Desing per il Made in Italy: Identità, Innovazione e Sostenibilità", administrative headquarter University of Campania "Luigi Vanvitelli", Caserta (Italy). We sincerely thank Prof. Chiara Zanardi and Dr. Giulia Cazzador from Ca' Foscari University of Venice for their valuable contribution in providing the SEM images. We would like to thank Dr. Silvia Conca (Crossing Srl) for reviewing the manuscript.

Author contributions D. Santandrea: Conceptualization, data curation, investigation, formal analysis, writing—original draft, review & editing. J. Caldato: Investigation and data curation. V. Beghetto: Conceptualization, formal analysis, writing—review & editing, fund raising.

Funding National Recovery and Resilience Plan (PNRR), for the 38th PhD cycle "National Interest PhD Program in Design for Made in Italy: Identity, Innovation,and Sustainability", administrative headquarter University of Campania "Luigi Vanvitelli", Caserta (Italy)

Data availability No datasets were generated or analysed during the current study.

Declarations

Competing interest The authors declare no competing interests.

References

Ali N, Katsouli J, Marczylo EL, Gant TW, Wright S, de la Serna JB (2024) The potential impacts of micro-and-nano plastics on various organ systems in humans. EBioMedicine 99:10490. https://doi.org/10.1016/j.ebiom.2023.104901

Plastics Industry Association, homepage. https://www.plasticsindustry.org/. Accessed 26/03/2025.

Basak S, Dangate MS, Samy S (2024) Oil-and water-resistant paper coatings: a review. Prog Org Coat 186:107938. https://doi.org/10.1016/j.porgcoat.2023.107938

Basta AH, Khwaldia K, Aloui H, El-Saied H (2015) Enhancing the performance of carboxymethyl cellulose by chitosan in producing barrier coated paper sheets. NPPRJ 30(4):617–625. https://doi.org/10.3183/npprj-2015-30-04-p617-625

Beghetto V, Agostinis L, Gatto V, Samiolo R, Scrivanti A (2019) Sustainable use of 4-(4, 6-dimethoxy-1, 3, 5-triazin-2-yl)-4-methylmorpholinium chloride as metal free tanning agent. J Clean Prod 220:864–872. https://doi.org/10.1016/j.jclepro.2019.02.034

Beghetto V, Gatto V, Conca S, Bardella N, Buranello C, Gasparetto G, Sole R (2020) Development of 4-(4, 6-dimethoxy-1, 3, 5-triazin-2-yl)-4-methyl-morpholinium chloride cross-linked carboxymethyl cellulose films. Carb Pol 249:116810. https://doi.org/10.1016/j.carbpol.2020.116810

Bendahou A, Hajlane A, Dufresne A, Boufi S, Kaddami H (2015) Esterification and amidation for grafting long aliphatic chains on to cellulose nanocrystals: a comparative study. Res Chem Intermed 41:4293–4310. https://doi.org/10.1007/s11164-014-1530-z

Borke T, Winnik FM, Tenhu H, Hietala S (2015) Optimized triazine-mediated amidation for efficient and controlled functionalization of hyaluronic acid. Carbohydr Polym 116:42–50. https://doi.org/10.1016/j.carbpol.2014.04.012

Charpentier D, Mocanu G, Carpov A, Chapelle S, Merle L, Müller G (1997) New hydrophobically modified carboxymethylcellulose derivatives. Carb Pol 33(2–3):177–186. https://doi.org/10.1016/S0144-8617(97)00031-3

Charpentier-Valenza D, Merle L, Mocanu G, Picton L, Muller G (2005) Rheological properties of hydrophobically modified carboxymethylcelluloses. Carb Pol 60(1):87–94. https://doi.org/10.1016/j.carbpol.2004.11.030

Cozens EJ, Roohpour N, Gautrot JE (2021) Comparative adhesion of chemically and physically crosslinked poly (acrylic acid)-based hydrogels to soft tissues. Eur Polym J 146:110250. https://doi.org/10.1016/j.eurpolymj.2020.110250

D'Este M, Eglin D, Alini M (2014) A systematic analysis of DMTMM vs EDC/NHS for ligation of amines to hyaluronan in water. Carb Pol 108:239–246. https://doi.org/10.1016/j.carbpol.2014.02.070

de Lima Santos K, Moraes GH, Nolêtto APR, do Amaral Sobral PJ (2024) Biopolymer-based coatings containing active ingredients for cellulosic packaging: a review. Cellulose 31(13):7841–7863. https://doi.org/10.1007/s10570-024-06039-9

El-Sayed S, Mahmoud KH, Fatah AA, Hassen ADSC (2011) DSC, TGA and dielectric properties of carboxymethyl cellulose/polyvinyl alcohol blends. Phys b: Condens Matter 406(21):4068–4076. https://doi.org/10.1016/j.physb.2011.07.050

European Parliament and Council. (1994). *Directive 94/62/EC on packaging and packaging waste*. Official Journal of the European Union, L 365, 31 December 1994, pp. 10–23. Retrieved from https://eur-lex.europa.eu/legal-content/EN/TXT/?uri=CELEX:32019D0665

Geyer R, Jambeck JR, Law KL (2017) Production, use, and fate of all plastics ever made. Sci Adv 3(7):e1700782. https://doi.org/10.1126/sciadv.1700782

Ghanbarzadeh B, Almasi H, Entezami AA (2010) Physical properties of edible modified starch/carboxymethyl cellulose films. IFSET 11(4):697–702. https://doi.org/10.1016/j.ifset.2010.06.001

Hassani FZSA, Salim MH, Kassab Z, Sehaqui H, Ablouh EH, Bouhfid R, Qaiss AEL, El Achaby M (2022) Crosslinked starch-coated cellulosic papers as alternative food-packaging materials. RSC Adv 12(14):8536–8546. https://doi.org/10.1039/D2RA00536K

He Y, Li H, Fei X, Peng L (2021) Carboxymethyl cellulose/cellulose nanocrystals immobilized silver nanoparticles as an effective coating to improve barrier and antibacterial properties of paper for food packaging applications. Carb Pol 252:117156. https://doi.org/10.1016/j.carbpol.2020.117156

Heinze T & Pfeiffer K (1999). Studies on the synthesis and characterization of carboxymethylcellulose. Appl Macromol Chem Phys, 266(1): 37–45. https://doi.org/10.1002/(SICI)1522-9505(19990501)266:1<37::AID-APMC37>3.0.CO;2-Z

Heydari A, Borazjani N, Kazemi-Aghdam F, Filo J, Lacík I (2025) DMTMM-mediated amidation of sodium alginate in aqueous solutions: pH-dependent efficiency of conjugation. Carb Pol 348:122893. https://doi.org/10.1016/j.carbpol.2024.122893

Hickman TJ, Tao L, Stingelin N, Meredith JC (2024) Low-water-permeability foils based on bio-renewable cellulose derivatives. RSC Sustain. https://doi.org/10.1039/D4SU00425F

Ho FF, Klosiewicz DW (1980) Proton nuclear magnetic resonance spectrometry for determination of substituents and their distribution in carboxymethylcellulose. Anal Chem 52(6):913–916. https://doi.org/10.1021/ac50056a032

Kim HJ, Roy S, Rhim JW (2021) Effects of various types of cellulose nanofibers on the physical properties of the CNF-based films. J Environ Chem Eng 9(5):106043. https://doi.org/10.1016/j.jece.2021.106043

Kobayashi J, Kaneko M, Supachettapun C, Takada K, Kaneko T, Kim JY, Ishida M, Kawai M, Mitsumata T (2023) Mechanical properties and reinforcement of paper sheets composited with carboxymethyl cellulose. Polymers 16(1):80. https://doi.org/10.3390/polym16010080

Kobayashi J, Kaneko M, Supachettapun C, Takada K, Kaneko T, Kim JY, Ishida M, Kawai M, Mitsumata T (2024) Mechanical properties and reinforcement of paper sheets composited with carboxymethyl cellulose. Polymers 16(1):80. https://doi.org/10.3390/polym16010080

Koppolu R, Lahti J, Abitbol T, Aulin C, Kuusipalo J, Toivakka M (2023) Tailoring the performance of nanocellulose-based multilayer-barrier paperboard using biodegradable-thermoplastics, pigments, and plasticizers. Cellulose 30(11):6945–6958. https://doi.org/10.1007/s10570-023-05281-x

Kunam PK, Ramakanth D, Akhila K, Gaikwad KK (2024) Bio-based materials for barrier coatings on paper packaging. Biomass Conv Biorefin 14(12):12637–12652. https://doi.org/10.1007/s13399-022-03241-2

Kunishima M, Kawachi C, Monta J, Terao K, Iwasaki F, Tani S (1999) 4-(4, 6-dimethoxy-1, 3, 5-triazin-2-yl)-4-methylmorpholinium chloride: an efficient condensing agent leading to the formation of amides and esters. Tetrahedron 55(46):13159–13170. https://doi.org/10.1016/S0040-4020(99)00809-1

Lavoine N, Desloges I, Khelifi B, Bras J (2014) Impact of different coating processes of microfibrillated cellulose on the mechanical and barrier properties of paper. J Mater Sci 49:2879–2893. https://doi.org/10.1007/s10853-013-7995-0

Lavoine N, Bras J, Saito T, Isogai A (2016) Improvement of the thermal stability of tempo-oxidized cellulose nanofibrils by heat-induced conversion of ionic bonds to amide bonds. Macromol Rapid Commun 37(13):1033–1039. https://doi.org/10.1002/marc.201600186

Lavrič G, Zamljen A, Juhant Grkman J, Jasiukaitytė-Grojzdek E, Grilc M, Likozar B, Gregor-Svetec D, Vrabič-Brodnjak U (2021) Organosolv lignin barrier paper coatings from waste biomass resources. Polymers 13(24):4443. https://doi.org/10.3390/polym13244443

Le Gars M, Delvart A, Roger P, Belgacem MN, Bras J (2020) Amidation of TEMPO-oxidized cellulose nanocrystals using aromatic aminated molecules. Colloid Polym Sci 298:603–617. https://doi.org/10.1007/s00396-020-04640-5

Li W, Wang S, Wang W, Qin C, Wu M (2019) Facile preparation of reactive hydrophobic cellulose nanofibril film for reducing water vapor permeability (WVP) in packaging applications. Cellulose 26:3271–3284. https://doi.org/10.1007/s10570-019-02270-x

Li Z, Rabnawaz M, Khan B (2020) Response surface methodology design for biobased and sustainable coatings for water-and oil-resistant paper. ACS Appl Polym Mater 2(3):1378–1387. https://doi.org/10.1021/acsapm.9b01238

Luo D, Chu X, Wu Y, Wang Z, Liao Z, Ji X, Ju J, Yang B, Chen Z, Dahlgren R, Zhang M, Shang X (2024) Micro-and

nano-plastics in the atmosphere: a review of occurrence, properties and human health risks. J Hazard Mater. https://doi.org/10.1016/j.jhazmat.2023.133412

Mazhari Mousavi SM, Afra E, Tajvidi M, Bousfield DW, Dehghani-Firouzabadi M (2017) Cellulose nanofiber/carboxymethyl cellulose blends as an efficient coating to improve the structure and barrier properties of paperboard. Cellulose 24:3001–3014. https://doi.org/10.1007/s10570-017-1299-5

Mishra, V., & Kumar, R. (**2012**). Graft copolymerization of Carboxymethylcellulose: an Overview. *Trends Carbohydr Res*, 4(3).

Mu C, Guo J, Li X, Lin W, Li D (2012) Preparation and properties of dialdehyde carboxymethyl cellulose crosslinked gelatin edible films. Food Hydrocoll 27(1):22–29. https://doi.org/10.1016/j.foodhyd.2011.09.005

Mujtaba M, Lipponen J, Ojanen M, Puttonen S, Vaittinen H (2022) Trends and challenges in the development of bio-based barrier coating materials for paper/cardboard food packaging; a review. Sci Total Environ 851:158328. https://doi.org/10.1016/j.scitotenv.2022.158328

Ni S, Zhang H, Dai H, Xiao H (2018) Starch-based flexible coating for food packaging paper with exceptional hydrophobicity and antimicrobial activity. Polymers 10(11):1260. https://doi.org/10.3390/polym10111260

Nongnual T, Butprom N, Boonsang S, Kaewpirom S (2024) Citric acid crosslinked carboxymethyl cellulose edible films: a case study on preserving freshness in bananas. Int J Biol Macromol 267:131135. https://doi.org/10.1016/j.ijbiomac.2024.131135

Pescheux-Sergienko J, Sillard C, Belgacem MN, Bras J (2024) Simultaneous comminution and hydrophobization of cellulose fibers by mechanochemistry. ACS Sustain Chem Eng 12(45):16540–16552. https://doi.org/10.1021/acssuschemeng.4c04209

Pettignano A, Charlot A, Fleury E (2019a) Carboxyl-functionalized derivatives of carboxymethyl cellulose: towards advanced biomedical applications. Pol Rev 59(3):510–560. https://doi.org/10.1080/15583724.2019.1579226

Pettignano A, Charlot A, Fleury E (2019b) Solvent-free synthesis of amidated carboxymethyl cellulose derivatives: effect on the thermal properties. Polymers 11(7):1227. https://doi.org/10.3390/polym11071227

Putri RDA, Setiawan A, Anggraini PD (2017) Effect of carboxymethyl cellulose (CMC) as biopolymers to the edible film sorghum starch hydrophobicity characteristics. In AIP Conference Proceedings 1818:1. https://doi.org/10.1063/1.4976908

Rachtanapun P, Luangkamin S, Tanprasert K, Suriyatem R (2012) Carboxymethyl cellulose film from durian rind. LWT - Food Sci Technol 48(1):52–58. https://doi.org/10.1016/j.lwt.2012.02.029

Rastogi VK, Samyn P (2015) Bio-based coatings for paper applications. Coatings 5(4):887–930. https://doi.org/10.3390/coatings5040887

Riaz A, Lagnika C, Luo H, Nie M, Dai Z, Liu C, Song J (2020) Effect of Chinese chives (*Allium tuberosum*) addition to carboxymethyl cellulose based food packaging films. Carb Pol 235:115944. https://doi.org/10.1016/j.carbpol.2020.115944

Richard CM, Dejoie E, Wiegand C, Gouesbet G, Colinet H, Balzani P, Siaussat D, Renault D (2024) Plastic pollution in terrestrial ecosystems: current knowledge on impacts of micro and nano fragments on invertebrates. J Hazard Mater. https://doi.org/10.1016/j.jhazmat.2024.135299

Santandrea D, Sillard C, Beghetto V, Bras J (2025) Aqueous-phase surface amidation of TEMPO-CNF films for improved adsorption of organic pollutants in water. ChemPlusChem 15:20. https://doi.org/10.1002/cplu.202500398

dos Santos Lima KT, de Matos Fonseca J, Monteiro AR, Valencia GA (2025) Progress in biopolymer coatings for achieving sustainable paper and paperboard packaging for food applications: a brief review. Packag Technol Sci 38(2):109–116. https://doi.org/10.13039/501100003593

Shimizu M, Saito T, Fukuzumi H, Isogai A (2014) Hydrophobic, ductile, and transparent nanocellulose films with quaternary alkylammonium carboxylates on nanofibril surfaces. Biomacromol 15(11):4320–4325. https://doi.org/10.1021/bm501329v

Šimkovic I, Gucmann F, Hricovíni M, Mendichi R, Schieroni AG, Piovani D, Zappia S, Dobročka E, Filip EJ, Hricovíni M (2023) Properties of quaternized and crosslinked carboxymethylcellulose films. Cellulose 30(4):2023–2036. https://doi.org/10.1007/s10570-022-05031-5

Solala I, Bordes R, Larsson A (2018) Water vapor mass transport across nanofibrillated cellulose films: effect of surface hydrophobization. Cellulose 25(1):347–356. https://doi.org/10.1007/s10570-017-1608-z

Sole R, Gatto V, Conca S, Bardella N, Morandini A, Beghetto V (2021) Sustainable triazine-based dehydro-condensation agents for amide synthesis. Molecules 26(1):191. https://doi.org/10.3390/molecules26010191

Sole R, Buranello C, Di Michele A, Beghetto V (2022) Boosting physical-mechanical properties of adipic acid/chitosan films by DMTMM cross-linking. Int J Biol Macromol 209:2009–2019. https://doi.org/10.1016/j.ijbiomac.2022.04.181

Standard Test Method for Water Vapor Transmission of Materials. (2017). ASTM E96–95. https://www.astm.org/e0096-95.html. Accessed: 07/03/2025

Swarupa S, Thareja P (2024) Techniques, applications and prospects of polysaccharide and protein based biopolymer coatings: a review. Int J Biol Macromol. https://doi.org/10.1016/j.ijbiomac.2024.131104

Tanpichai S, Witayakran S, Wootthikanokkhan J, Srimarut Y, Woraprayote W, Malila Y (2020) Mechanical and antibacterial properties of the chitosan coated cellulose paper for packaging applications: Effects of molecular weight types and concentrations of chitosan. Int J Biol Macromol 155:1510–1519. https://doi.org/10.1016/j.ijbiomac.2019.11.128

Tardy BL, Richardson JJ, Greca LG, Guo J, Bras J, Rojas OJ (2023) Advancing bio-based materials for sustainable solutions to food packaging. Nat Sustain 6(4):360–367. https://doi.org/10.1038/s41893-022-01012-5

Taubner T, Synytsya A, Čopíková J (2015) Preparation of amidated derivatives of carboxymethylcellulose. Int J Biol Macromol 72:11–18. https://doi.org/10.1016/j.ijbiomac.2014.07.049

Tavares KM, de Campos A, Luchesi BR, Resende AA, de Oliveira JE, Marconcini JM (2020) Effect of carboxymethyl cellulose concentration on mechanical and water vapor barrier properties of corn starch films. Carbohydr Polym 246:116521. https://doi.org/10.1016/j.carbpol.2020.116521

Teisala H, Tuominen M, Kuusipalo J (2014) Superhydrophobic coatings on cellulose-based materials: fabrication, properties, and applications. Adv Mater Interfaces 1(1):1300026. https://doi.org/10.1002/admi.201300026

Thompson, K. F. (2005). Modification of polymeric substrates using surface-grafted nanoscaffolds. Georgia Institute of Technology.

UNEP - UN Environmental Program Homepage (2020). https://www.unep.org/interactives/beat-plastic-pollution/. Accessed 22/03/2025

Yook S, Park H, Park H, Lee SY, Kwon J, Youn HJ (2020) Barrier coatings with various types of cellulose nanofibrils and their barrier properties. Cellulose 27:4509–4523. https://doi.org/10.1007/s10570-020-03061-5

Yoshikawa Y, Yamato K, Ishida A, Yoshida Y, Kumamoto Y, Isogai A (2025) Amidation of carboxy groups in TEMPO-oxidized cellulose for improving surface hydrophobization and thermal stability of TEMPO-CNCs. Carb Pol 347:122654. https://doi.org/10.1016/j.carbpol.2024.122654

Zabivalova NM, Bochek AM, Kalyuzhnaya LM, Vlasova EN, Volchek BZ (2003) Carboxymethyl cellulose amides and their properties. Russ J Appl Chem 76:1998–2002. https://doi.org/10.1023/B:RJAC.0000022456.23088.b6

Zhai Z, Zhou Y, Korovich AG, Hall BA, Yoon HY, Yao Y, Zhang J, Bortner MJ, Roman M, Madsen LA, Edgar KJ (2023) Synthesis and characterization of multi-reducing-end polysaccharides. Biomacromol 24(6):2596–2605. https://doi.org/10.1021/acs.biomac.3c00104

Zhang S, Li W, Wang W, Wang S, Qin C (2019) Reactive superhydrophobic paper from one-step spray-coating of cellulose-based derivative. Appl Surf Sci 497:143816. https://doi.org/10.1016/j.apsusc.2019.143816

Zhang J, Guo Z, Chen S, Dong H, Zhang X, Qin Y, Yao C, Xu F (2021) High-barrier, strong, and antibacterial paper fabricated by coating acetylated cellulose and cinnamaldehyde for food packaging. Cellulose 28:4371–4384. https://doi.org/10.1007/s10570-021-03778-x

Zhang J, Youngblood JP (2025) Cellulose nanofibril-based hybrid coatings with enhanced moisture barrier properties. Mat Adv. https://doi.org/10.1039/D4MA01276C

Zolfi M, Khodaiyan F, Mousavi M, Hashemi M (2014) Development and characterization of the kefiran-whey protein isolate-TiO2 nanocomposite films. Int J Biol Macromol 65:340–345. https://doi.org/10.1016/j.ijbiomac.2014.01.010